Sound of Fermi arcs: a linearly dispersing gapless surface plasmon mode in undoped Weyl semimetals

F. Adinehvand, Z. Faraei, T. Farajollahpour, and S. A. Jafari [*]

Department of Physics, Sharif University of Technology, Tehran 11155-9161, Iran

Using Green's function of semi-infinite Weyl semimetals, we present the quantum theory of the collective charge dynamics of Fermi arcs. We find that the Fermi arc plasmons in *undoped* Weyl semimetals are linearly dispersing gapless plasmon modes. The gaplessness comes from proper consideration of the deep penetration of surface states near the end of the Fermi arcs into the interior of the Weyl semimetal. The linear dispersion— rather than square root dispersion of *pure 2D* electron systems with extended Fermi surface—arises from the strong anisotropy introduced by the Fermi arc itself, due to which the continuum of surface particle-hole (PH) excitations in this system will have a strong resemblance to a stack of one-dimensional (1D) electron systems. This places the Fermi arc electron liquid in between the 1D and 2D electron liquids. Contamination with the bulk PH excitations in the *doped case* gives rise to the damping of the Fermi arc sounds.

I. INTRODUCTION

The excitation spectrum of electronic systems in atomic length scales is composed of individual electrons, while beyond a certain length scale, their collective character becomes manifest [1–3]. Among the salient collective excitations in electron liquids are plasmon which are collective density oscillations [2] that appear as poles in the density-density correlation function [4] and depend on space dimension. A simple and generic hydrodynamic approach [5] captures the essential features of plasmons: In three dimensions (3D) they are always gapped and are given by $\omega_{p,3D}^2 \sim ne^2/\epsilon_0 m$ [1,6]. In two dimensions (2D) they get softer and disperse as $\propto \sqrt{q}$. This holds for 2D materials with quadratic band dispersion [4] as well as for Dirac dispersion [7,8]. The gaplessness is ideal for subwavelength optics [9]. 2D plasmons were first observed in a sheet of electrons on liquid helium [10,11] and then in inversion layers [12], and a metallic surface-state band [13], as well as in graphene [14]. A natural place to look for 2D plasmons is the surface of 3D systems. The resulting surface plasmons explain the energy loss of fast electrons passing through thin films [15]. Since the penetration depth of electromagnetic waves in metals is rather short, the plasmons of metal surfaces are major players in technical applications of the collective oscillations [9,16–20].

On the other hand, in one dimension (1D) the fixed point of interacting conducting electron systems is the Luttinger liquid [21], rather than a Fermi liquid [22]. The low-energy sector of the spectrum of interacting fermion systems in 1D is exhausted by collective excitations only. The collective charge density excitations appear in the form of linearly dispersing sound waves [23–25]. This can be simply understood in Fig. 1 by comparison of the PH continuum (PHC) of 1D (a) and 2D

(b) systems [26]. In 1D, the low-q part is composed of free PH excitations all moving at the *same group velocity*, such that any amount of Coulomb interaction binds them into coherent collective modes [26]. This is in contrast to the PHC of higher dimensional electron gases with an extended Fermi surface in Fig. 1(b) where due to rotational freedom of the wave vector $\boldsymbol{q}$, there is no coherence in the group velocity of the PH pairs [4]. Therefore, the electron liquids in dimensions higher than one cannot sustain acoustic plasmon excitations. In the presence of at least one more layered 2D electron gas [27], the coupling of the individual plasmons in various layers can always generate an in-phase linearly dispersing plasmon wave [28]. Such a composite double-layer plasmon has been observed on the Be (0001) surface [29]. But this never happens for an *isolated* 2D system. Another way to get a higher dimensional linear plasmon concerns a genuine nonequilibrium situation recently proposed for the bulk of 3D Weyl semimetals [30].

In this work we will show that the electron gas formed by Fermi arc states on the surface of Weyl semimetals (WSMs) supports a linearly dispersing gapless plasmon mode. To see how this can happen, imagine a momentum space stack of 1D system whose PHC can be obtained by uniformly translating the PHC in Fig. 1(a) which results in Fig. 1(c). In doing so, the essential feature, namely a constant phase velocity at small q, is preserved. The Fermi arcs actually correspond to "one-half" of this picture as they can be imagined to arise from stacks of chiral QH states [31] in the momentum space [32,33]. In that sense they correspond to collections of 1D problems. This gives rise to PHC of Fermi arcs shown in Fig. 1(d), resembling the low-q side of Fig. 1(c).[1]

---

[1]Note that for Fermi arcs, the portion of PHC that touches the $\omega = 0$ line at $2k_F$ is absent. Because the separation between the right- and left-moving Fermi arcs in the momentum axis is zero.
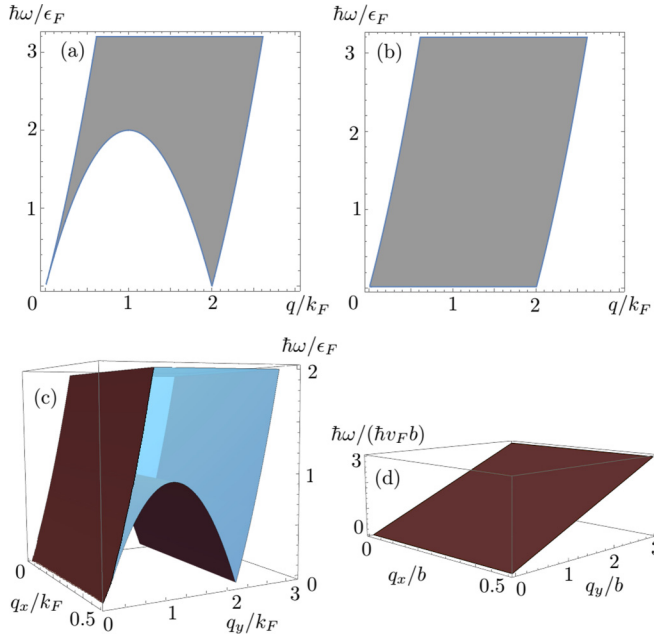
*jafari@physics.sharif.edu

FIG. 1. PHC in (a) 1D and (b) 2D electron gases. (c) PHC of a momentum space stack of 1D systems. The scale $2k_F$ is separation of left and right movers in momentum space. (d) PHC of Fermi arc. Panel (d) coincides with low-q part of (c).
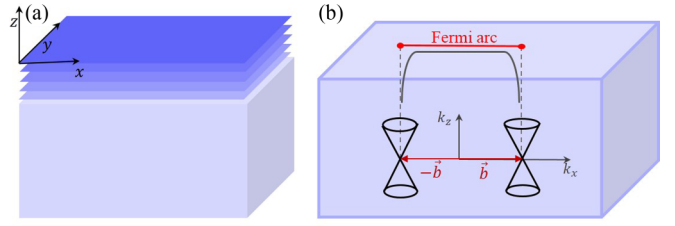

FIG. 2. (a) Schematic representation of the semi-infinite WSM. Color intensity encodes the exponential decay of the surface states. The layers represent the discretization of the z coordinate used in numerical computation. (b) The Fermi arc on the surface of a Weyl semimetal that connects the projection of two Weyl nodes on the surface. The gray curve denotes the penetration depth of the Fermi arc states into the interior of the WSM.

The bulk electronic states in WSMs [33–35] is composed of linearly dispersing bands that touch each other at nodal points [36,37]. WSMs are materials realization of axion electrodynamics [38,39]. WSMs are characterized by very peculiar surface states known as Fermi arcs [40] which are localized on the surface if the Fermi wave vector is in the middle of the arc, but penetrate deeply into the bulk as the (Fermi) wave vector approaches the two ends of the Fermi arc [41]. Bulk plasmons and their associated surface plasmon resonance (resulting from the projection of dielectric function on the surface) have been studied in WSMs [42,43]. In these systems the gapped plasmon in the 3D plasmons is given by $\sim e^2 n^{2/3} v_F$.

Previous attempts to study the collective charge dynamics are as follows: Using the assumption of specular reflection of incident electrons—equivalent to projection of the bulk dielectric function to the $z = 0$ boundary surface—Lošić obtained gapped surface plasmon resonances for doped Weyl semimetals [44]. Employing a simple dispersion of Fermi arcs, and neglecting the associated matrix elements, Lošić found a plasmon mode dispersing as $\sqrt{q_y} = \sqrt{q \sin \theta}$ (y direction is perpendicular to the Fermi arc). Apart from the angular dependence, the $\sqrt{q}$ behavior is expected for an *isolated* 2D system with an *extended Fermi surface*. Andolina and co-workers have studied the same problem [43]. If only the contribution of arc states is taken into account, the plasmons for the Fermi arc states in their work becomes gapped. Song and Rudner employed a classical electrodynamics for doped WSM and found a branch of surface plasmons as merely arising from the boundary condition [45]. Their work was followed by Gorbar and co-workers [46] who studied the surface collective modes. In both works the bulk of the

WSM is assumed to be doped and is characterized by a bulk plasmon frequency ω_{pl}. In such a case the projection of the Fermi surfaces of bulk and the surface Fermi arc merge and form closed banana-shaped surfaces [47]. The extreme case is however the undoped limit where the bulk Fermi surface and its associated bulk plasmons go away, and one is left with a pure Fermi arc collective dynamics. In this case, the banana-shaped Fermi surfaces will reduce to a line segment properly dubbed Fermi arc. In this paper we are interested in the quantum theory of the Fermi arc plasmons in undoped WSM.

Using the Green's function approach [41] we find that the deep penetration of end-of-Fermi-arc states into the bulk, combined with the peculiar form of PHC in Fig. 1(d), will compromise to produce a gapless branch of linearly dispersing Fermi arc plasmons. Let us briefly elaborate on these points: (i) As can be seen in Fig. 2(b), the penetration length of Fermi arc states into the interior of the WSM increases by approaching the two ends of Fermi arcs. The authors of Ref. [43] project the polarization function onto the surface, and avoid dealing with a determinantal equation in real-space coordinates z, z'. Evading the determinant misses the long tail of Fermi arc states. We will show how systematic treatment of the penetration effect by progressively increasing the size of the determinant involved, gives rise to gapless plasmon mode. (ii) The Fermi arc *per se*, creates enormous anisotropy in such a way that the phase space for PH processes in Fig. 1(d) will resemble those of the assembly of one-dimensional systems as depicted in Fig. 1(c). This is in sharp contrast to the systems with extended closed Fermi surface where a rotational freedom of the wave vector $\boldsymbol{q}$ of low-energy scattering processes gives rise to a PHC of type (b) rather than type (c) in Fig. 1. In this way the resulting plasmon mode will become a (linearly dispersing) sound wave. Note that such a Fermi arc sound wave is categorically different from the chiral zero sound (CZS) introduced in Ref. [30] in the following respects: (i) To generate the CZS one needs to generate a *nonequilibrium* population around the right and left Weyl nodes. (ii) To realize the CZS the intervalley relaxation rate must be much smaller than intravalley timescales. (iii) Realization of *chiral* zero sound requires a background B field to generate right/left movers, i.e., it is built on the chiral anomaly.

II. MODEL AND FORMALISM

We consider a semi-infinite WSM in $z < 0$ part of the space bounded by $z = 0$ surface as in Fig. 2(a). In our previous works [41,48] we have used the Green's function approach to formulate the Fermi arcs. We do not assume any particular Hamiltonian for the Fermi arc states. Rather, we obtain the Fermi arcs from appropriate *boundary conditions* [41]. In this way, we ensure that all the necessary matrix elements, as well as the tail of Fermi arc states in the bulk (see Fig. 2), are properly taken into account. The deep penetration of the states near the ends of the Fermi arc into the interior of WSM is one of the essential differences of the electron gas formed by the Fermi arc with respect to the standard 2D electron gases. Missing this effect will give rise to $\sqrt{q}$ behavior [44] of the standard 2D electron gas systems.

When the translational symmetry along the z axis is broken by the presence of a surface at $z = 0$, the dielectric function will become a matrix in spatial z, z' indices. The "dielectric matrix" in the random phase approximation is given by

$$\varepsilon_{z,z'}(q, \omega) = 1 - V_{z,z'}(q)\Pi_{z,z'}(q, \omega), \qquad (1)$$

where $V_{z,z'}(\vec{q}) = 2\pi e^2 e^{-q|z-z'|}/q$ is the Coulomb matrix element with $\vec{q} = (q_x, q_y)$ denoting the wave vector in the plane. Here z and z' are the distance of the two electrons from the boundary. When they are at the same plane, $z = z'$, this reduces to the Coulomb matrix element of the 2D systems [49]. $\Pi_{z,z'}(\vec{q}, \omega)$ is the polarizability tensor which can be written in terms of the Green's function as

$$\Pi_{z,z'}(\vec{q}, \omega) = \sum_{\vec{k}, \nu} G_{z,z'}(\vec{k}, \nu)G_{z',z}(\vec{k} + \vec{q}, \omega + \nu). \qquad (2)$$

From this point we do not perform any further approximations such as projection of the polarization function into the surface [44] or approximating the determinants such as $\det \varepsilon_{z,z'} = 0$ by a related trace operation [43]. Instead, following Andersen

and co-workers [50] the plasmon resonance in a generic situation with a broken translation invariance are numerically obtained. For this purpose, one needs to numerically solve the eigenvalue equation,

$$\int \varepsilon(\boldsymbol{r}, \boldsymbol{r}', \omega)\phi_n(\boldsymbol{r}', \omega)d\boldsymbol{r}' = \varepsilon_n(\omega)\phi_n(\boldsymbol{r}, \omega), \qquad (3)$$

and then to find zero eigenvalues $\varepsilon_n(\omega) = 0$. By scanning a range of ω values, one can find the energy scales ω_p at which the eigenvalues of the dielectric matrix vanish, $\varepsilon_n(\omega_p) = 0$. This will correspond to plasmon resonances. Various branches are labeled by n. We are interested in the lowest energy branch. Furthermore, at a resonance the loss function $\text{Im}(\varepsilon_n^{-1})$ will develop a peak which corresponds to the characteristic energy losses suffered by fast charged particles traversing the material [51]. To take the long penetration depth of Fermi arc states into account, one needs to discretize the portion of space near the surface as depicted in Fig. 2. The separation between the Weyl nodes is $2|\vec{b}|$, where b is used as a unit of momentum (also sets the unit of length as $\hbar/b$).

To calculate the $\varepsilon(\boldsymbol{r}, \boldsymbol{r}', \omega)$, one basically needs the polarization function $\Pi(\boldsymbol{r}, \boldsymbol{r}', \omega)$ as they are related by Eq. (B1). In the geometry of Fig. 2, the translational symmetry in (x, y) plane, reduces the polarization to $\Pi(z, z', \boldsymbol{q}, \omega)$ where $\boldsymbol{q} = (q_x, q_y)$ is the in-plane wave vector. To calculate the polarization we can use the Green's functions obtained for the Weyl Hamiltonian. As we are interested in bare Fermi arc plasmons, we use the part of the Green's functions corresponding to surface degrees of freedom which are naturally separated from the bulk part [41]. Without loss of generality, we rotate the coordinate system, such that the Fermi arc is oriented on the k_x axis. In this situation the Green's function will become much easier to work with [48]. Convolution of the Green's functions (which are 2×2 matrices in their spin indices) as in Eq. (2) gives (see Appendix A for details),

$$
\begin{aligned}
\Pi_{z,z'}^{\uparrow\uparrow/\downarrow\downarrow} &= \frac{e^{-b\zeta}q_y}{4\pi^4\zeta^3(\omega - q_y)}\{\sinh(q_x\zeta/2)[b\zeta^2\cosh b\zeta - (\zeta + b\zeta^2)\sinh b\zeta](2q_x \mp iq_y) \\
&\quad + \cosh(q_x\zeta/2)[(4b^2\zeta^2 + 4 + 4b\zeta \mp iq_xq_y\zeta^2)\sinh\zeta b - (4b\zeta + 4b^2\zeta^2)\cosh b\zeta]\}, \\
\Pi_{z,z'}^{\uparrow\downarrow/\downarrow\uparrow} &= \frac{e^{-b\zeta}q_y}{4\pi^4\zeta^3(\omega - q_y)}\{\sinh(q_x\zeta/2)[(q_xq_y\zeta^2 \mp 4i\zeta b \mp 4i\zeta^2b^2 \mp 4i)\sinh\zeta b \pm (4i\zeta^2b^2 + 4i\zeta b)\cosh b\zeta] \\
&\quad + \cosh(q_x\zeta/2)[-(\zeta + b\zeta^2)\sinh\zeta b + b\zeta^2\cosh\zeta b](q_y \mp 2iq_x)\},
\end{aligned}
\qquad (4)
$$

where $2\vec{b} = (2b, 0, 0)$ is the vector that connects the Weyl nods in the bulk of the WSM and $\zeta = 2(z + z')$ with z and z' measured from the surface. The dispersion of Fermi arc states involves single particles moving along positive y direction on the top surface shown in Fig. 2. Therefore PH excitations with positive energy are restricted to $q_y > 0$ on the surface shown. However, *in reality* there is always another surface in the other side referred to as the bottom surface in the following (not shown in the geometry of Fig. 2). The bottom surface contains the $q_y < 0$ portion of PH excitations. A nice property of the above polarization matrix elements is that under mirror reflection with respect to Fermi arc, $\varphi \rightarrow -\varphi$ or $q_y \rightarrow -q_y$

(equivalent to going from top surface to bottom surface), we have $\Pi^{\alpha\beta}(q, \varphi, \omega) \rightarrow \alpha\beta\Pi^{\bar{\alpha}\bar{\beta}}(q, -\varphi, -\omega)$, where α, β can take the values $\uparrow \equiv +1$ or $\downarrow \equiv -1$.

To solve for $\det \varepsilon = 0$, we need to discretize the z direction in Eq. (4) and form the $\Pi_{z,z'}^{\alpha,\beta}$ matrix. Discretization by a mesh of size N, we will be dealing with $2N \times 2N$ matrices, where the factor of 2 comes from the above matrix structure in the spin space. The numerical details are given in Appendix B. To develop a first feeling about the Fermi arc plasmon dispersion, let us start with the $N = 1$ approximation which can be analytically handled. In this case, we just need to consider one layer at $z = 0$. Equation (B1) for one layer
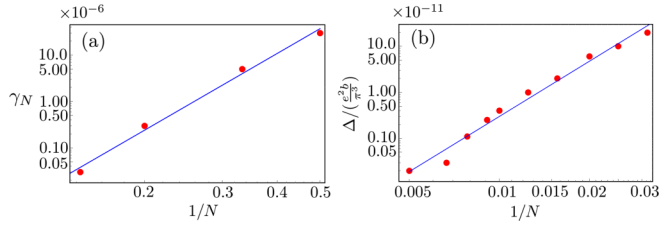
FIG. 3. Finite size scaling analysis of the relative slope difference γ_N (left) and the gap Δ_N (right) of the lowest Fermi arc plasmon modes. The log-log plot indicates that upon increasing N the gap and slope differences quickly vanish.

gives

$$\varepsilon = \begin{pmatrix} 1 - V_0\Pi^{\uparrow\uparrow} & -V_0\Pi^{\uparrow\downarrow} \\ -V_0\Pi^{\downarrow\uparrow} & 1 - V_0\Pi^{\downarrow\downarrow} \end{pmatrix}, \tag{5}$$

where $V_0 = V_{z=0,z'=0}(q) = 2\pi e^2/q$ is a pure 2D Coulomb interaction matrix element. In the $q \to 0$ limit, the determinant of the above dielectric matrix has the following zeros which after restoring various constants gives the following q-linear plasmon dispersion:

$$\hbar\omega = \hbar q v_F \sin\varphi(1 \pm \gamma_1) + \Delta_1, \tag{6}$$

where $\gamma_1 = \alpha_{\text{WSM}}\sqrt{\sin^2\varphi + 4\cos^2\varphi}/(2\pi^2)$ is the (dimensionless) relative difference in the slope of two modes and is determined by the "fine structure" constant $\alpha_{\text{WSM}} = e^2/(\hbar v_F)$ which is of the order of unity for Fermi velocities. The gap for $N = 1$ approximation is given by $\Delta_1 = \frac{2e^2 b}{\pi^3}\sin\varphi$. But the two-dimensional electron systems cannot have gapped plasmons [4,49]. In fact, anticipating that γ and Δ will depend on the mesh size N, we have introduced subscript "1" in γ_1 and Δ_1. To investigate this systematically, in Fig. 3 we study the effect of taking progressively deeper layers around the surface into account. As can be seen, by increasing N both γ_N (left panel) and Δ_N (right panel) approach zero. This figure clearly shows that the gap $\Delta_{N=1}$ and the slope difference $\gamma_{N=1}$ are artifacts of considering a mesh of size $N = 1$ and quickly vanish by taking progressively larger mesh sizes into account. As pointed out, this form of finite size effect arises because the states at the two ends of the Fermi arc deeply penetrate into the bulk as in Fig. 2. The conclusion is that the numerical evaluation of the determinant of ε for reasonably large N cannot be avoided. Evading this determinant by projecting it to the surface—which might be valid for typical non-Weyl electronic systems—introduces severe errors in the dispersion of Fermi arc plasmons [43,44].

Although the $N = 1$ approximation to determinant of ε does not give correct gap and slope, the linear nature of the plasmon dispersion and its angular dependence survive the larger N limit. To establish the linear q dependence and $\sin\varphi$ angular dependence, in Fig. 4 we have plotted the dispersion of the (doubly degenerate) lowest plasmon mode for large enough $N = 50$ to ensure that γ_N and Δ_N are already zero. The direction of the wave vector $\boldsymbol{q}$ is fixed by $\varphi = \pi/6$ where $\varphi = \arctan(q_y/q_x)$ is the polar angle of $\boldsymbol{q}$. Note that in this figure both ω and $\boldsymbol{q}$ are plotted in their natural units. As can be seen, the linear dispersion of the $N = 1$ approximation, surprisingly robust at much larger N. Extrapolating the dispersion
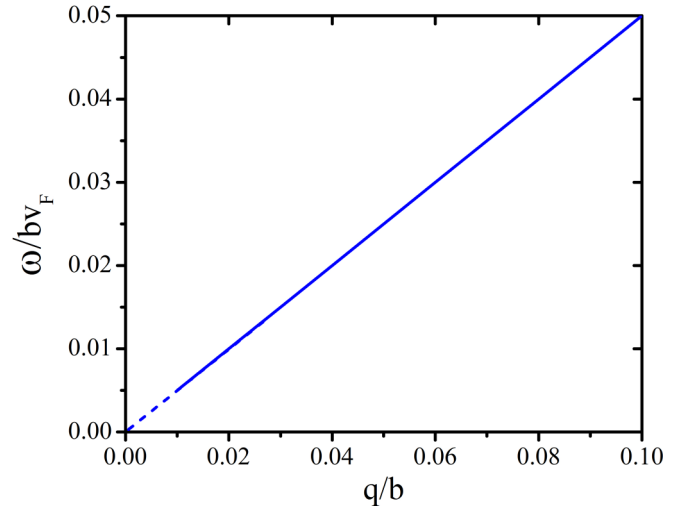

FIG. 4. Lowest surface plasmon mode of Fermi arc states for a grid of $N = 50$ layers with penetration depth of $db = 25$. The polar angle is fixed by $\varphi = \pi/6$. The dashed line emphasizes the extrapolation to $q \to 0$ limit.

to $q \to 0$ limit clearly confirms that for this value of mesh size, the plasmon mode is gapless. Also the fact that in Fig. 3 the relative slope difference γ_N is already zero for $N = 50$ indicates that this lowest mode is doubly degenerate. The double degeneracy corresponds to $\uparrow$ and $\downarrow$ spin directions.

The remaining task is to investigate the angular dependence of the linear plasmon mode of the Fermi arcs. The slope of the lowest Fermi arc plasmon mode in Fig. 4 is (within the machine precision) given by $\sin(\pi/6) = 0.5$. To explore this further, in Fig. 5 we have plotted the lowest mode plasmon frequency as a function of the polar angle φ for a fixed $|\boldsymbol{q}| = 0.01b$. The magnitude of wave vector has been chosen small enough to ensure that it already lies in the linear dispersion regime. The dashed line denotes the numerical data, while the solid line represents the $\sin\varphi$ profile. Please note that the $\sin\varphi$ angular dependence is also robust in the limit of larger mesh sizes. Therefore properly handling the penetration of Fermi arc states into the interior of WSM gives rise to a branch of linear plasmon mode which is doubly (spin) degenerate and disperses as $\omega = v_F q \sin\varphi = v_F q_y$. The linear dispersion is in agreement with the hydrodynamic result of Song and Rudner [45]. When the doping in their work is set to zero by sending the bulk Drude weight $\mathcal{D}$ and bulk plasmon frequency and
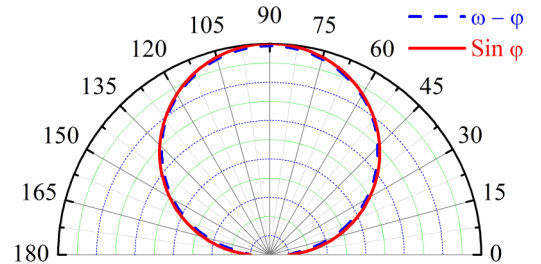

FIG. 5. The lowest surface plasmon frequency (dashed blue) and $\sin\varphi$ function (solid red) as a function of the polar angle φ for $N = 50$ and $db = 25$ for a fixed $q = 0.01b$ wave vector magnitude.
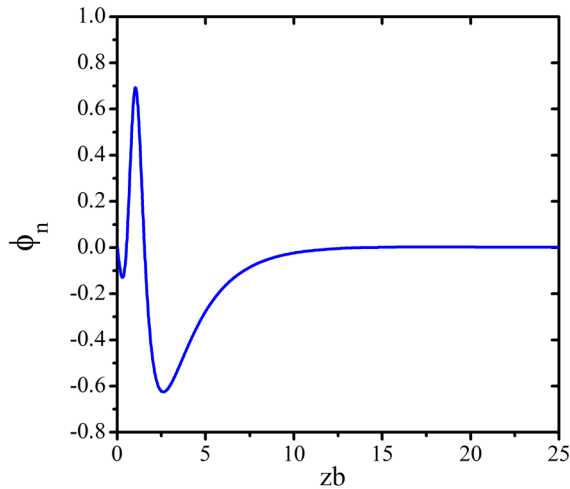
FIG. 6. The electrostatic potential profile for spin ↑ and ↓ (degenerate) Fermi arc electrons as a function of distance zb from the surface for $\varphi = \pi/6$, $|q| = 0.1$, and $N = 150$. The modes are localized on the surface.

the nonuniversal bulk Hall conductance to zero, indeed one recovers a linearly dispersing solution to the surface plasmon (note that the x direction in the above work is the same as y direction in our work). Our work in addition to being a quantum mechanical extension of Ref. [45], clarifies that the gaplessness is connected with the deep penetration of the Fermi arc particle states into the interior of WSM.

Finally, in Fig. 6 we have plotted the eigenfunctions of Eq. (3) that correspond to zeros of the dielectric function $\varepsilon_n(\omega)$. The eigenfunction corresponds to lowest mode evaluated for parameters $N = 150$ and $db = 75$ and $q = 0.1b$. For such a large value of N the slope difference γ_N is already zero, and this electrostatic profile is doubly degenerate corresponding to ↑ and ↓ spin densities. The actual density of electrons according to Poisson equation will be the second derivative of this curve. The mode is clearly bound to the surface of the WSM.

III. FERMI ARC AS A UNIQUE ELECTRON LIQUID

Typically for an extended Fermi surface in 2D, one expects a $\sqrt{q}$ plasmon dispersion. But the linear plasmon $q \sin \varphi = q_y$ arising from the Fermi arc states (of undoped WSMs) is in sharp contrast to the usual 2D plasmons. Even more surprising is the fact that this behavior does not receive any correction by numerically computing the plasmons for larger N. So there must be a reason for this behavior. To elaborate on this, let us start by noting that apart from diploar $\sin \varphi$ angular dependence (which is a 2D feature), the linear sound mode is reminiscent of the 1D bosonic modes. Indeed, due to strong anisotropy of the Fermi arc, the PHC of Fermi arc states in Fig. 1(d) bears more resemblance to the PHC of a collection of 1D systems in Fig. 1(c), rather than the PHC of 2D systems in Fig. 1(b).

If the dispersion $\varepsilon(k_y) = k_y$ of the Fermi arc was a 1D dispersion, then a straightforward bosonization argument [24] would give the charge bosonic collective mode with $\omega(q_y) \propto q_y$ dispersion. The dispersion of Fermi arc states is quite

similar, $\varepsilon^{\mathrm{arc}}(\boldsymbol{k}) = k_y$, albeit with the important difference that k_y is now a component of a 2D vector $\boldsymbol{k} = (k_x, k_y)$. The restricted phase space for the bosonic mode formation in Fig. 1(c) within the random phase approximation gives the bosonic mode $\omega(\boldsymbol{q}) \sim q_y = |\boldsymbol{q}| \sin \varphi$. The excellent fit of the numerical data obtained from RPA dielectric matrix suggest that the anisotropy of the Fermi arc states is likely to admit interesting forms of bosonization which may allow one to go far beyond our simple RPA treatment. From this point of view, the electron gas formed by the Fermi arc states is actually something between 1D and 2D. The peculiar 1D-like PHC of the Fermi arc plasmons will protect them from Landau damping into the surface PH excitations. However, contamination with the *bulk* PHC of excitations which is expected to be stronger for those Fermi arc states closer to the ends of Fermi arc can lead to the damping of Fermi arc plasmon sounds.

IV. SUMMARY AND DISCUSSION

Within the random phase approximation, we studied the collective charge dynamics of the Fermi arc states of undoped Weyl semimetals. Fermi arc states near the projection of Weyl nodes have infinite localization lengths. Proper treatment of these tails by considering large enough grids makes the collective excitations gapless and the ↑ and ↓ modes degenerate. Failing to account for this long tail, will generate gapped plasmons [42,43] for pure Fermi arc states. The peculiar spectrum of Fermi arc states places them somewhere in between the 1D and 2D electron liquids (Fig. 1). As such, unlike the typical 2D electron liquids with extended Fermi surface for which the plasmon disperses as $\sqrt{q}$, for the Fermi arcs we find a plasmon branch dispersing as $q \sin \varphi$ where φ is the polar angle of the wave-vector $\boldsymbol{q}$ with respect to the arc direction [45]. The linear dispersion is more like a 1D feature which arises from the limited phase space for PH excitations in Fig. 1(d). This peculiar PHC endows the Fermi arc states with a sound branch arising from density oscillations of the electrons in the charge channel. The $\sin \varphi$ angular dependence is the only effect of the second space dimension. Given the 1D analogy, one expects an interesting spin mode in these systems as well [24,52–54]. Unlike the chiral zero sound of bulk electronic degrees of freedom in Weyl semimetals [30], the present sound is due to Fermi arcs states *in equilibrium*. Contamination with bulk PHC in doped systems damps the sound mode [43].

APPENDIX A: POLARIZABILITY

In this Appendix we give the details of the calculation of the charge polarizability given in Eq. (4) of the main text. The polarizability $\Pi(\vec{q}, \omega)$ can be expressed in terms of the

chirality diagonal Green's function as follows:

$$\Pi^{\uparrow\uparrow}(\vec{q}, \omega) = \sum_{\chi} \sum_{\vec{k}, \nu} [G^{\uparrow\uparrow}(\vec{k} + \vec{q}, \nu + \omega)G^{\uparrow\uparrow}(\vec{k}, \nu) + G^{\uparrow\downarrow}(\vec{k} + \vec{q}, \nu + \omega)G^{\downarrow\uparrow}(\vec{k}, \nu)],$$

$$\Pi^{\uparrow\downarrow}(\vec{q}, \omega) = \sum_{\chi} \sum_{\vec{k}, \nu} [G^{\uparrow\uparrow}(\vec{k} + \vec{q}, \nu + \omega)G^{\uparrow\downarrow}(\vec{k}, \nu) + G^{\uparrow\downarrow}(\vec{k} + \vec{q}, \nu + \omega)G^{\downarrow\downarrow}(\vec{k}, \nu)],$$

$$\Pi^{\downarrow\uparrow}(\vec{q}, \omega) = \sum_{\chi} \sum_{\vec{k}, \nu} [G^{\downarrow\downarrow}(\vec{k} + \vec{q}, \nu + \omega)G^{\downarrow\uparrow}(\vec{k}, \nu) + G^{\downarrow\uparrow}(\vec{k} + \vec{q}, \nu + \omega)G^{\uparrow\uparrow}(\vec{k}, \nu)],$$

$$\Pi^{\downarrow\downarrow}(\vec{q}, \omega) = \sum_{\chi} \sum_{\vec{k}, \nu} [G^{\downarrow\downarrow}(\vec{k} + \vec{q}, \nu + \omega)G^{\downarrow\downarrow}(\vec{k}, \nu) + G^{\downarrow\uparrow}(\vec{k} + \vec{q}, \nu + \omega)G^{\uparrow\downarrow}(\vec{k}, \nu)],$$

$$\text{(A1)}$$

where $\chi = \pm 1$ refers to chirality which corresponds to right/left-handed fermions in WSMs, and $\sum_{\vec{k}}$ understood to mean $\int\int dk_x dk_y/(2\pi)^2$ and the integration range is $-q_y < k_y < 0$, $-b < k_x < b$ defining the chiral Fermi arc on the (top) surface. The Green's function is given by (for more details please see Ref. [41])

$$G^{\bar{\sigma}\sigma}_{\chi\chi'}(z, z') = C^{\bar{\sigma}\sigma}_{\chi\chi'}(z')e^{-(q_\chi + i\chi b_z)z} - \frac{\chi\left(k_x^\chi + i\sigma k_y^\chi\right)}{8\pi^2(q_\chi + i\chi b_z)}e^{-(q_\chi + i\chi b_z)|z-z'|}\delta_{\chi\chi'},$$

$$G^{\sigma\sigma}_{\chi\chi'}(z, z') = \frac{\varepsilon - i\chi\sigma\partial_z + \sigma b_z}{\chi\left(k_x^\chi + i\sigma k_y^\chi\right)}G^{\bar{\sigma}\sigma}_{\chi\chi'}(z, z').$$

$$\text{(A2)}$$

Coefficient $C^{\bar{\sigma}\sigma}_{\chi\chi'}(z')$ is specified by the boundary condition. Here we choose the boundary condition that the boundary does not mix the chiralities. Then in this situation we have

$$C^{\bar{\sigma}\sigma}_{\chi\chi}(z') = \frac{\varepsilon - i\chi\sigma q_\chi + 2\sigma b_z - \chi e^{-i\sigma\theta_\chi}\left(k_x^\chi + i\sigma k_y^\chi\right)}{\varepsilon + i\chi\sigma q_\chi - \chi e^{-i\sigma\theta_\chi}\left(k_x^\chi + i\sigma k_y^\chi\right)} \frac{\chi\left(k_x^\chi + i\sigma k_y^\chi\right)}{8\pi^2(q_\chi + i\chi b_z)}.$$

$$\text{(A3)}$$

Here we assume that the Fermi arc is on the k_x axis and lies between $-b$ to b. For simplicity, we break polarization function to two part, and define $\Pi^{\uparrow\uparrow}(q, \omega, z, z')$ as

$$\Pi^{\uparrow\uparrow}(\vec{q}, \omega, z, z') = \Pi_1^{\uparrow\uparrow}(\vec{q}, \omega, z, z') + \Pi_2^{\uparrow\uparrow}(\vec{q}, \omega, z, z'), \tag{A4}$$

where

$$\Pi_1^{\uparrow\uparrow}(\vec{q}, \omega, z, z') = \int dk_x \int dk_y \sum_{\nu\chi} G^{\uparrow\uparrow}(\vec{k} + \vec{q}, \nu + \omega)G^{\uparrow\uparrow}(\vec{k}, \nu)$$

$$= \left(\frac{2}{8\pi^2}\right)^2 \int dk_x \int dk_y \sum_{\nu\chi} \frac{b - \chi(k_x + q_x) - i\chi(k_y + q_y)}{\nu + \omega - k_y - q_y} \frac{b - \chi k_x - i\chi k_y}{\nu - k_y}e^{-(2b - 2\chi k_x - \chi q_x)(z+z')}$$

$$= \left(\frac{2}{8\pi^2}\right)^2 \int dk_x \int dk_y \sum_{\chi} \frac{(b - \chi k_x - \chi q_x - i\chi k_y - i\chi q_y)(b - \chi k_x - i\chi k_y)}{\omega - q_y}e^{(-2b + \chi q_x)(z+z')}e^{2\chi k_x(z+z')}$$

$$= \left(\frac{2}{8\pi^2}\right)^2 \int dk_x \int_{-q_y}^{0} dk_y \sum_{\chi} \frac{e^{(-2b + \chi q_x)(z+z')}}{\omega - q_y}\big[b^2 - 2\chi b k_x - i\chi b k_y + k_x^2$$

$$+ ik_x k_y - \chi q_x b + q_x k_x + iq_x k_y - ib\chi k_y + ik_x k_y - k_y^2 - i\chi b q_y + iq_y k_x - q_y k_y\big]e^{2\chi k_x(z+z')}$$

$$= \left(\frac{2}{8\pi^2}\right)^2 \sum_{\chi} \frac{e^{(-2b + \chi q_x)(z+z')}}{\omega - q_y}\int_{-b}^{b} dk_x e^{2\chi k_x(z+z')}\big\{[b^2 - 2\chi b k_x + k_x^2 - \chi q_x b + q_x k_x - i\chi b q_y + iq_y k_x]k_y$$

$$+ k_y^2/2[-2i\chi b + 2ik_x + iq_x - q_y] - k_y^3/3\big\}\big|_{-q_y}^{0}$$

$$= \left(\frac{2}{8\pi^2}\right)^2 \sum_{\chi} \frac{e^{(-2b + \chi q_x)(z+z')}}{\omega - q_y}\int_{-b}^{b} dk_x\big\{q_y k_x^2 + k_x[-2\chi b q_y + q_x q_y] + b^2 q_y - \chi b q_x q_y - iq_x q_y^2/2 + q_y^3/6\big\}e^{2\chi k_x(z+z')}$$

$$= \left(\frac{2}{8\pi^2}\right)^2 \sum_{\chi} \frac{e^{(-2b + \chi q_x)(z+z')}}{\omega - q_y}\bigg\{[b^2 q_y - \chi b q_x q_y - iq_x q_y^2/2 + q_y^3/6]\frac{2}{\eta}\sinh(b\eta)$$

$$+[-2\chi bq_y + q_xq_y]\left[\frac{2b}{\eta}\cosh(b\eta) - \frac{2}{\eta^2}\sinh(b\eta)\right] + q_y\left[\frac{2b^2}{\eta}\sinh(b\eta) - \frac{4b}{\eta^2}\cosh(b\eta) + \frac{4}{\eta^3}\sinh(b\eta)\right]\Big\}\quad\text{(A5)}$$

and

$$\Pi_2^{\uparrow\uparrow}(\vec{q},\omega,z,z') = \int dk_x \int dk_y \sum_{\nu\chi} G^{\downarrow\uparrow}(\vec{k}+\vec{q},\nu+\omega)G^{\uparrow\downarrow}(\vec{k},\nu)$$

$$= \left(\frac{2}{8\pi^2}\right)^2 \int dk_x \int dk_y \sum_{\nu\chi} \frac{(k_x+q_x-\chi b+ik_y+iq_y)(k_x-\chi b-ik_y)}{(\nu+\omega-k_y-q_y)(\nu-k_y)}e^{-(2b-2\chi k_x-\chi q_x)(z+z')}$$

$$= \left(\frac{2}{8\pi^2}\right)^2 \sum_{\chi} \frac{e^{(-2b+\chi q_x)(z+z')}}{\omega-q_y} \int_{-b}^{b} dk_x e^{2\chi k_x(z+z')}\Big\{\big[k_x^2-2\chi bk_x+q_xk_x-\chi bq_x+b^2+iq_yk_x-i\chi bq_y\big]k_y$$

$$+ [-iq_x+q_y]k_y^2/2 + k_y^3/3\big\}\Big|_{-q_y}^{0}$$

$$= \left(\frac{2}{8\pi^2}\right)^2 \sum_{\chi} \int_{-b}^{b} dk_x \Big\{k_x^2 q_y + \big[-2\chi bq_y + q_xq_y + iq_y^2\big]k_x$$

$$+ \big[-\chi bq_xq_y + b^2q_y - i\chi bq_y^2 + iq_xq_y^2/2 - q_y^3/6\big]e^{2\chi k_x(z+z')}\Big\}$$

$$= \left(\frac{2}{8\pi^2}\right)^2 \sum_{\chi} \frac{e^{(-2b+\chi q_x)(z+z')}}{\omega-q_y}\Big\{\big[b^2q_y - \chi bq_xq_y - i\chi bq_y^2 + iq_xq_y^2/2 - q_y^3/6\big]\frac{2}{\eta}\sinh(b\eta)$$

$$+ [-2\chi bq_y + q_xq_y + iq_y^2]\left[\frac{2b}{\eta}\cosh(b\eta) - \frac{2}{\eta^2}\sinh(b\eta)\right] + q_y\left[\frac{2b^2}{\eta}\sinh(b\eta) - \frac{4b}{\eta^2}\cosh(b\eta) + \frac{4}{\eta^3}\sinh(b\eta)\right]\Big\},$$

$$\text{(A6)}$$

where $\eta = \chi\zeta = 2\chi(z+z')$, and after performing the $\sum_{\chi=\pm1}$ we obtain

$$\Pi^{\uparrow\uparrow} = Ae^{q_x(z+z')}\Big\{2q_y\left[\frac{2b^2}{\zeta}\sinh(b\zeta) - \frac{4b}{\zeta^2}\cosh(b\zeta) + \frac{4}{\zeta^3}\sinh(b\zeta)\right] + \left[\frac{2b}{\zeta}\cosh(b\zeta) - \frac{2}{\zeta^2}\sinh(b\zeta)\right](-4bq_y+2q_xq_y-iq_y^2)$$

$$+ [2b^2q_y - 2bq_xq_y - iq_xq_y^2 + ibq_y^2]\frac{2}{\zeta}\sinh(b\zeta)\Big\}$$

$$+ Ae^{-q_x(z+z')}\Big\{2q_y\left[\frac{2b^2}{\zeta}\sinh(b\zeta) - \frac{4b}{\zeta^2}\cosh(b\zeta) + \frac{4}{\zeta^3}\sinh(b\zeta)\right] - \left[\frac{2b}{\zeta}\cosh(b\zeta) - \frac{2}{\zeta^2}\sinh(b\zeta)\right](4bq_y+2q_xq_y-iq_y^2)$$

$$+ [2b^2q_y + 2bq_xq_y - iq_xq_y^2 - ibq_y^2]\frac{2}{\zeta}\sinh(b\zeta)\Big\}$$

$$= A\sinh[q_x(z+z')]\Big\{\left[\frac{2b}{\zeta}\cosh(b\zeta) - \frac{2}{\zeta^2}\sinh(b\zeta)\right](2q_xq_y-iq_y^2) + \big[-2bq_xq_y + ibq_y^2\big]\frac{2}{\zeta}\sinh(b\zeta)\Big\}$$

$$+ A\cosh[q_x(z+z')]\Big\{q_y\left[\frac{4b^2}{\zeta}\sinh(b\zeta) - \frac{8b}{\zeta^2}\cosh(b\zeta) + \frac{8}{\zeta^3}\sinh(b\zeta)\right] + \frac{2}{\zeta}\sinh(b\zeta)[2b^2q_y - iq_xq_y^2]$$

$$- 4bq_y\left[\frac{2b}{\zeta}\cosh(b\zeta) - \frac{2}{\zeta^2}\sinh(b\zeta)\right]\Big\}.\quad\text{(A7)}$$

The coefficient A is defined by $A = \frac{e^{-b\zeta}}{8\pi^4(\omega-q_y)}$. After some simplification, we get to the following equation [the first part of Eq. (4) of the main text]:

$$\Pi^{\uparrow\uparrow(\downarrow\downarrow)}(\vec{q},\omega,z,z') = \frac{e^{-b\zeta}q_y}{4\pi^4\zeta^3(\omega-q_y)}\{\sinh(q_x\zeta/2)[b\zeta^2\cosh b\zeta - (\zeta+b\zeta^2)\sinh b\zeta](2q_x\mp iq_y)$$

$$+ \cosh(q_x\zeta/2)\big[(4b^2\zeta^2 + 4 + 4b\zeta \mp iq_xq_y\zeta^2)\sinh\zeta b - (4b\zeta + 4b^2\zeta^2)\cosh b\zeta\big]\}.\quad\text{(A8)}$$

For the second part of the Eq. (4) of the main text we have

$$\Pi^{\downarrow\uparrow}(\vec{q},\omega,z,z') = \sum_{\chi}\sum_{\vec{k},\nu}[G^{\downarrow\downarrow}(\vec{k}+\vec{q},\nu+\omega)G^{\downarrow\uparrow}(\vec{k},\nu) + G^{\downarrow\uparrow}(\vec{k}+\vec{q},\nu+\omega)G^{\uparrow\uparrow}(\vec{k},\nu)].\quad\text{(A9)}$$

Again we define the polarization function into two parts where

$$\Pi_1^{\downarrow\uparrow}(\vec{q}, \omega, z, z') = \sum_{\chi} \sum_{\vec{k},\nu} G^{\downarrow\downarrow}(\vec{k} + \vec{q}, \nu + \omega) G^{\downarrow\uparrow}(\vec{k}, \nu)$$

$$= \frac{2i\chi(k_y + q_y - i\chi b + ik_x + iq_x)}{8\pi^2(i\omega_n + i\nu_n - k_y - q_y)} \frac{-2i(k_x - \chi b + ik_y)}{8\pi^2(i\omega_n - k_y)} e^{-(2b - 2\chi k_x - \chi q_x)(z+z')}$$

$$= \frac{4\chi e^{(-2b + \chi q_x)(z+z')}}{(8\pi^2)^2(i\nu - q_y)} \int_{-b}^{b} dk_x \int_{-q_y}^{0} dk_y \{ k_y(k_X - \chi b) + ik_y^2 + (q_y - i\chi b + ik_x + iq_x)k_x$$

$$\times (q_y - i\chi_b + ik_x + iq_x)(-\chi b + ik_y) \} e^{2\chi k_x(z+z')}$$

$$= \frac{4\chi e^{(-2b + \chi q_x)(z+z')}}{(8\pi^2)^2(i\nu - q_y)} \int_{-b}^{b} dk_x \left\{ iq_y k_x^2 + (q_y^2 - 2i\chi bq_y + iq_x q_y)k_x + \left(-\frac{q_y^3}{6} + ib^2 q_y - i\chi bq_x q_y + \frac{q_x q_y^2}{2} - \chi bq_y^2 \right) \right\} e^{\eta k_x}$$

$$= \frac{4\chi e^{(-2b + \chi q_x)(z+z')}}{(8\pi^2)^2(i\nu - q_y)} \left\{ \left(\frac{2}{\eta} b \cosh \eta b - \frac{2}{\eta^2} b \sinh \eta b \right) (q_y^2 - 2i\chi bq_y + iq_x q_y) \right.$$

$$\left. + \frac{2}{\eta} \sinh \eta b \left(-\frac{iq_y^3}{6} + ib^2 q_y - i\chi bq_x q_y + \frac{q_x q_y^2}{2} - \chi bq_y^2 \right) + iq_y \left(\frac{2b^2}{\eta} \sinh \eta b - \frac{4b}{\eta^2} \cosh \eta b + \frac{4}{\eta^3} \sinh \eta b \right) \right\} \tag{A10}$$

and

$$\Pi_2^{\downarrow\uparrow}(\vec{q}, \omega, z, z') = \sum_{\chi} \sum_{\vec{k},\nu} G^{\downarrow\uparrow}(\vec{k} + \vec{q}, \nu + \omega) G^{\uparrow\uparrow}(\vec{k}, \nu)$$

$$= \frac{-2i\chi(k_x + q_x - i\chi b + ik_y + iq_y)}{8\pi^2(\omega + \nu - k_y - q_y)} \frac{-2i(k_y + i\chi b - ik_x)}{8\pi^2(\nu - k_y)} e^{-(2b - 2\chi k_x - \chi q_x)(z+z')}$$

$$= \frac{4\chi e^{(-2b + \chi q_x)(z+z')}}{(8\pi^2)^2(\omega - q_y)} \int_{-b}^{b} dk_x \int_{-q_y}^{0} dk_y \{ -k_y(k_x + p_x + ip_y - \chi b) - ik_y^2$$

$$+ (iq_y - \chi b + k_x + q_x)(-i\chi b + ik_x) + k_y(\chi b - k_y) \} e^{2\chi k_x(z+z')}$$

$$= \frac{4\chi e^{(-2b + \chi q_x)(z+z')}}{(8\pi^2)^2(\nu - q_y)} \int_{-b}^{b} dk_x \left\{ iq_y k_x^2 + i(-2\chi bq_y + q_x q_y)k_x + \left(i\frac{q_y^3}{6} + ib^2 q_y - i\chi bq_x q_y + \frac{q_x q_y^2}{2} \right) \right\} e^{\eta k_x}$$

$$= \frac{4\chi e^{(-2b + \chi q_x)(z+z')}}{(8\pi^2)^2(\nu - q_y)} \left\{ \left(\frac{2}{\eta} b \cosh \eta b - \frac{2}{\eta^2} b \sinh \eta b \right) (-2i\chi bq_y + iq_x q_y) \right.$$

$$\left. + \frac{2}{\eta} \sinh \eta b \left(\frac{iq_y^3}{6} + ib^2 q_y - i\chi bq_x q_y + \frac{q_x q_y^2}{2} \right) + iq_y \left(\frac{2b^2}{\eta} \sinh \eta b - \frac{4b}{\eta^2} \cosh \eta b + \frac{4}{\eta^3} \sinh \eta b \right) \right\}. \tag{A11}$$

Then using

$$\Pi^{\downarrow\uparrow}(\vec{q}, \omega, z, z') = \sum_{\chi = \pm 1} [\Pi_1^{\downarrow\uparrow}(\vec{q}, \omega, z, z') + \Pi_2^{\downarrow\uparrow}(\vec{q}, \omega, z, z')], \tag{A12}$$

we obtain

$$\Pi^{\downarrow\uparrow}(\vec{q}, \omega, z, z') = \frac{e^{-b\zeta}}{4\pi^4(\omega - q_y)} \left\{ \left[\left(\frac{2b}{\eta} \cosh \eta b - \frac{2}{\eta^2} \right)(q_y^2 + 2iq_x q_y) + \frac{2}{\eta} \sinh \eta b(-2ibq_x q_y - bq_y^2) \right] \cosh q_z(z+z') \right.$$

$$+ \left[\frac{2}{\eta} \sinh \eta b(2ib^2 q_y + q_x q_y) - 4ibq_y \left(\frac{2b}{\eta} \cosh \eta b - \frac{2}{\eta^2} \sinh \eta b \right) \right.$$

$$\left. \left. + iq_y \left(\frac{4b^2}{\eta} \sinh \eta b - \frac{8b}{\eta^2} \cosh \eta b + \frac{8}{\eta^3} \sinh \eta b \right) \right] \sinh q_x(z+z') \right\}. \tag{A13}$$

After some simplification we get [second part of Eq. (4) of the main text]

$$\Pi^{\uparrow\downarrow(\downarrow\uparrow)}(\vec{q}, \omega, z, z') = \frac{e^{-b\zeta} q_y}{4\pi^4 \zeta^3(\omega - q_y)} \{ \sinh(q_x \zeta/2)[(q_x q_y \zeta^2 \mp 4i\zeta b \mp 4i\zeta^2 b^2 \mp 4i) \sinh \zeta b \pm (4i\zeta^2 b^2 + 4i\zeta b) \cosh b\zeta]$$

$$+ \cosh(q_x \zeta/2)[-(\zeta + b\zeta^2) \sinh \zeta b + b\zeta^2 \cosh \zeta b](q_y \mp 2iq_x) \}. \tag{A14}$$

APPENDIX B: PLASMON EIGENVALUES

In this Appendix, following Refs. [50,51] of the main text, we summarize how to solve the plasmon eigenvalue problem in confined geometries. Longitudinal modes are zeros of the dielectric function. In a generic situation corresponding to an arbitrary geometry, the dielectric function will be a function of two separate spatial coordinates r and r'. The longitudinal modes arise from zeros of the dielectric function which can be viewed as a matrix in indices r and r'. One therefore needs to finds the zero modes of the following equation:

$$\int \varepsilon(r, r', \omega)\phi_n(r', \omega)dr' = \varepsilon_n(\omega)\phi_n(r, \omega), \qquad \text{(B1)}$$

where n labels various modes, and we are searching for solutions where the eigenvalue $\varepsilon_n(\omega) = 0$. Since we do not know *a priori* at which frequencies the dielectric eigenvalues $\varepsilon_n(\omega)$ become zero, one has to scan a range of ω values to find where the real part of $\varepsilon_n(\omega)$ crosses the zero. To this end a suitably chosen mesh can be used to discretize the matrix $\varepsilon(r, r', \omega)$ for a given fixed ω. Then for any given ω, the eigenvalues of the above equation are obtained. Varying ω gives typical plots like Fig. 7.

For the present situation, the wave vector q in the (q_x, q_y) plane is a good quantum number to label the plasmons. However the translational invariance along z is lost and therefore the dielectric matrix will be a matrix in spatial indices z, z' for given values of q and ω. This can be used to generate Fig. 7 which are generated for a mesh of size $N = 50$. The red plots are the real parts of $\varepsilon_n(\omega)$ and the blue plots are the imaginary parts of the loss function $1/\varepsilon_n(\omega)$ measured in electron energy
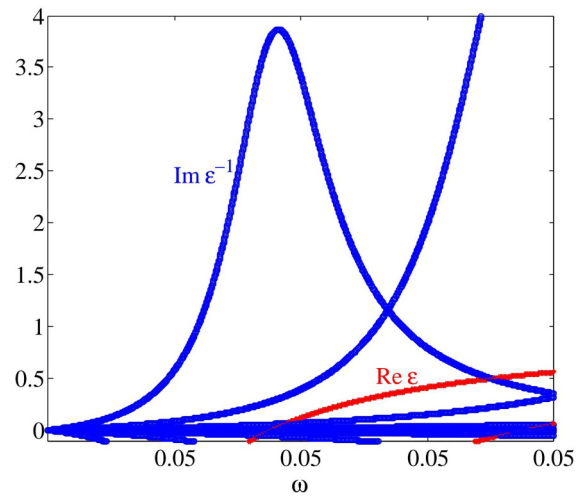

FIG. 7. The red plot is the real part of the eigenvalues $\varepsilon(\omega)$ of the dielectric matrix. The blue plot is the imaginary part of the loss function $\varepsilon^{-1}(\omega)$ as a function of frequency ω for a mesh with $N = 50$ layers and the horizontal momentum $q = 0.1$.

loss spectroscopy. Various plots correspond to various values of n. As can be seen in Fig. 7 the plasmon resonance is a frequency ω_p at which the real part of $\varepsilon_n(\omega)$ vanishes *and* the loss function $\text{Im}[\varepsilon_n^{-1}(\omega)]$ develops a peak.

Repeating the above procedure for all other values of q, allows us to map the dispersion of longitudinal (plasmon) modes. We are interested in the lowest $n = 0$ mode which are confined to the surface.

[1] P. Phillips, *Advanced Solid State Physics* (Cambridge University Press, Cambridge, 2012).

[2] D. Pines, *The Many-Body Problem* (Basic Books, New York, 1997).

[3] D. Bohm and D. Pines, Phys. Rev. **92**, 609 (1953).

[4] G. Giuliani and G. Vignale, *Quantum Theory of The Electron Liquid* (Cambridge University Press, Cambridge, 2005).

[5] S. A. Khan and M. Bonitz, *Complex Plasmas* (Springer, New York, 2014), pp. 103–152.

[6] C. Kittel *et al.*, *Introduction to Solid State Physics* (Wiley, New York, 1976), Vol. 8.

[7] E. H. Hwang and S. Das Sarma, Phys. Rev. B **80**, 205405 (2009).

[8] B. Wunsch, T. Stauber, F. Sols, and F. Guinea, New J. Phys. **8**, 318 (2006).

[9] W. L. Barnes, A. Dereux, and T. W. Ebbesen, Nature (London) **424**, 824 (2003).

[10] C. Grimes and G. Adams, Surf. Sci. **58**, 292 (1976).

[11] C. Grimes and G. Adams, Phys. Rev. Lett. **36**, 145 (1976).

[12] S. J. Allen, D. C. Tsui, and R. A. Logan, Phys. Rev. Lett. **38**, 980 (1977).

[13] T. Nagao, T. Hildebrandt, M. Henzler, and S. Hasegawa, Phys. Rev. Lett. **86**, 5747 (2001).

[14] A. Bostwick, T. Ohta, T. Seyller, K. Horn, and E. Rotenberg, Nat. Phys. **3**, 36 (2007).

[15] R. Ritchie and A. Marusak, Surf. Sci. **4**, 234 (1966).

[16] S. A. Maier and H. A. Atwater, J. Appl. Phys. **98**, 011101 (2005).

[17] G. E. Moore *et al.*, *Cramming More Components Onto Integrated Circuits* (McGraw-Hill, New York, 1965).

[18] E. Ozbay, Science **311**, 189 (2006).

[19] H. A. Atwater, Sci. Am. **296**, 56 (2007).

[20] J. Heber, Nat. News **461**, 720 (2009).

[21] J. Voit, Rep. Prog. Phys. **58**, 977 (1995).

[22] G. Baym and C. Pethick, *Landau Fermi-Liquid Theory* (Wiley, New York, 2004).

[23] D. Sénéchal, An introduction to bosonization, in *Theoretical Methods for Strongly Correlated Electrons* (Springer, Berlin, 2004), pp. 139–186.

[24] A. O. Gogolin, A. A. Nersesyan, and A. M. Tsvelik, *Bosonization and Strongly Correlated Systems* (Cambridge University Press, Cambridge, 2004).

[25] S. Rao and D. Sen, in *Field Theories in Condensed Matter Physics* (Springer, Berlin, 2001), pp. 239–333.

[26] T. Giamarchi, *Quantum Physics in One Dimension* (Clarendon, London, 2004).

[27] Z. Jalali-Mola and S. A. Jafari, Phys. Rev. B **98**, 235430 (2018).

[28] J.-J. Zhu, S. M. Badalyan, and F. M. Peeters, Phys. Rev. B **87**, 085401 (2013).

[29] B. Diaconescu, K. Pohl, L. Vattuone, L. Savio, P. Hofmann, V. M. Silkin, J. M. Pitarke, E. V. Chulkov, P. M. Echenique, D. Farías, and M. Rocca, Nature (London) **448**, 57 (2007).

[30] Z. Song and X. Dai, Phys. Rev. X **9**, 021053 (2019).

[31] L. Balents and M. P. A. Fisher, Phys. Rev. Lett. **76**, 2782 (1996).

[32] R.-J. Slager, V. Juričić, and B. Roy, Phys. Rev. B **96**, 201401(R) (2017).

[33] B. Yan and C. Felser, Annu. Rev. Condens. Matter Phys. **8**, 337 (2017).

[34] N. P. Armitage, E. J. Mele, and A. Vishwanath, Rev. Mod. Phys. **90**, 015001 (2018).

[35] S. Rao, arXiv:1603.02821.

[36] L. Lu, Z. Wang, D. Ye, L. Ran, L. Fu, J. D. Joannopoulos, and M. Soljačić, Science **349**, 622 (2015).

[37] S.-M. Huang, S.-Y. Xu, I. Belopolski, C.-C. Lee, G. Chang, B. Wang, N. Alidoust, G. Bian, M. Neupane, C. Zhang *et al.*, Nat. Commun. **6**, 7373 (2015).

[38] X.-L. Qi and S.-C. Zhang, Phys. Today **63**, 33 (2010).

[39] F. Wilczek, Phys. Rev. Lett. **58**, 1799 (1987).

[40] N. Xu, H. Weng, B. Lv, C. Matt, J. Park, F. Bisti, V. Strocov, D. Gawryluk, E. Pomjakushina, K. Conder *et al.*, Nat. Commun. **7**, 11006 (2016).

[41] Z. Faraei, T. Farajollahpour, and S. A. Jafari, Phys. Rev. B **98**, 195402 (2018).

[42] M. Lv and S.-C. Zhang, Int. J. Mod. Phys. B **27**, 1350177 (2013).

[43] G. M. Andolina, F. M. D. Pellegrino, F. H. L. Koppens, and M. Polini, Phys. Rev. B **97**, 125431 (2018).

[44] Ž. B. Lošić, J. Phys. Condens. Matter **30**, 365003 (2018).

[45] J. C. W. Song and M. S. Rudner, Phys. Rev. B **96**, 205443 (2017).

[46] E. V. Gorbar, V. A. Miransky, I. A. Shovkovy, and P. O. Sukhachov, Phys. Rev. B **99**, 155120 (2019).

[47] F. D. M. Haldane, arXiv:1401.0529.

[48] Z. Faraei and S. A. Jafari, Phys. Rev. B **100**, 035447 (2019).

[49] M. I. Katsnelson, *Graphene: Carbon in Two Dimension* (Cambridge University Press, Cambridge, 2012).

[50] K. Andersen, K. W. Jacobsen, and K. S. Thygesen, Phys. Rev. B **86**, 245129 (2012).

[51] K. T. Winther, Quantum theory of Plasmons in Nanostructures, Ph.D. thesis, Center for Atomic-scale Materials Design, Technical University of Denmark, Denmark, 2015.

[52] G. Baskaran and S. A. Jafari, Phys. Rev. Lett. **89**, 016402 (2002).

[53] G. Baskaran and S. A. Jafari, Phys. Rev. Lett. **92**, 199702 (2004).

[54] S. A. Jafari and G. Baskaran, J. Phys. Condens. Matter **24**, 095601 (2012).